Identification of Potential Anti-Inflammatory Phytochemicals Targeting Endothelial Protein C Receptor (EPCR) Through Molecular Docking and Molecular Dynamics Simulations

Aishwarya Jadhav[1], Dr. Elangbam Singh[2]*, Dr. Sagar Bhayye[3]

[1]PhD scholar, Department of Plant Biotechnology, Rajiv Gandhi Institute of I.T. and Biotechnology, Bharati Vidyapeeth (Deemed to be University) Katraj, Pune-411046, Maharashtra, India, Email ID: aishwarya.jadhav.ext@bharatividyapeeth.edu.

[2] Vice Principal, Department of Plant Biotechnology, Rajiv Gandhi Institute of I.T. and Biotechnology, Bharati Vidyapeeth (Deemed to be University) Katraj, Pune-411046, Maharashtra, India, Email id: elangbam.singh@bharatividyapeeth.edu

[3]Assistant Professor, Department of Bioinformatics, Rajiv Gandhi, Institute of I.T. and Biotechnology, Bharati Vidyapeeth (Deemed to be University), Katraj, Pune-411046, Maharashtra, India, Email ID: sagar.bhayye@bharatividyapeeth.edu

Corresponding Author

**Dr. Elangbam Singh (Ph.D), Vice Principal, Department of Plant Biotechnology, Rajiv Gandhi Institute of I.T. and Biotechnology, Bharati Vidyapeeth (Deemed to be University) Katraj, Pune-411046, Maharashtra, India, Email id: elangbam.singh@bharatividyapeeth.edu*

Abstract:

Inflammation is a key contributor to several chronic diseases, including rheumatoid arthritis, cardiovascular disorders, and cancer. The endothelial protein C receptor (EPCR) plays a crucial role in regulating inflammation and coagulation, making it a promising therapeutic target. In this study, a structure-based computational approach was used to identify potential anti-inflammatory phytochemicals targeting EPCR. A large phytochemical library from IMPPAT and COCONUT databases was screened, followed by ADMET filtering, resulting in 278 drug-like compounds for further analysis. Molecular docking identified four lead compounds (L10, L41, L111, and L114) with stronger binding affinities than the reference drug diclofenac. These compounds formed stable interactions with key EPCR residues through hydrogen bonding, hydrophobic contacts, and π–π stacking interactions. Molecular dynamics simulations over 200 ns confirmed the structural stability of the ligand–EPCR complexes, supported by favourable RMSD, RMSF, and free-energy profiles. MM-GBSA analysis further demonstrated superior binding energies for L114 (-32.20 ± 0.02 kcal/mol), L41 (-30.15 ± 0.02 kcal/mol), and L111 (-28.19 ± 0.02 kcal/mol) compared to diclofenac (-25.18 ± 0.03 kcal/mol). Among the screened compounds, L114 emerged as the most promising EPCR inhibitor. These findings suggest that selected phytochemicals, particularly L114, may serve as potential lead molecules for developing safer anti-inflammatory therapies targeting EPCR.

Keywords: Endothelial Protein C Receptor (EPCR), Anti-inflammatory Phytochemicals, Molecular Docking, Molecular Dynamics Simulation, Virtual Screening, lMM-GBSA Analysis, Drug Discovery

How to cite this article: Jadhav A, Singh E, Bhayye S. Identification of Potential Anti-Inflammatory Phytochemicals Targeting Endothelial Protein C Receptor (EPCR) Through Molecular Docking and Molecular Dynamics Simulations. Int J Drug Deliv Technol. 2026;16(64s):617-626. DOI: 10.25258/ijddt.16.64s.60

1. Introduction:

Inflammation is a tightly regulated by many biological processes and involved in pathophysiological conditions of neurodegenerative, cardiovascular, autoimmune, and metabolic diseases and disorders. The endothelin protein C receptor (EPCR) prominently binds to activated protein C (APC) pathway by forming thrombin-thrombomodulin (TM) complex which is playing important role in thrombosis (coagulation) and inflammation [Fukudome et al., 1994; Stearns-Kurosawa et al., 1996; Van de Wouwer et al., 2004; Esmon, 2004, 2006; Weiler, 2010; Xue and March, 2025]. The EPCR is expressed in various cell types such as vascular smooth muscle cells, eosinophils, neutrophils, monocytes, keratinocytes, along with fetal liver embryonic hematopoietic stem cells (HSCs), breast cancer stem cells and on the surface of bone marrow [Gleeson et al., 2012]. EPCR has been emerged as a pivotal factor in coagulation and inflammation and impacting the pathophysiological conditions of several diseases including rheumatoid arthritis (RA), malaria, cancer, inflammatory bowel disease (IBD) and hemophilia [Scaldaferri et al., 2007; Lust et al., 2008; Moxon et al., 2013; Mohan et al., 2014; Xue and March, 2025].

In addition, the high expression of EPCR was observed in lung cancer and hepatocellular carcinoma (HCC) and its association with carcinogenesis has been well documented [Biguzzi et al., 2007; Heng et al., 2013]. EPCR promotes cell migration, invasion, and angiogenesis and inhibit cell apoptosis in various subtypes of cancers [Beaulieu and Church, 2007; Mohan et al., 2014]. Further, EPCR is highly expressed in rheumatoid synovial fibroblasts (RASFs) and responsible for the inflammatory and cartilage-degradative actions, and aggressive behaviour of RASFs [Xue et al., 2014]. The suppression of EPCR through siRNA leads to reduction in inflammatory mediators interleukin-1-beta (IL-1β), cadherin-11, MAP kinases and NF-κB which subsequently supresses the cell viability, cell invasion and cartilage degradation in RASFs [Xue et al., 2014; Xue and March, 2025]. Therefore, it may be used as a biomarker for early detection of lung cancer and HCC [Mohan et al., 2014]. EPCR is involved in diverse functions associated with many pathophysiological conditions because of its ability to interacting with multiple ligands [Mohan et al., 2014]. Therefore, EPCR may serve as a promising therapeutic target to reduce inflammation, enhance endothelial function and mitigate the aggressive behaviour of RASF, and lower the risk of thrombosis and CVD in RA patients [Van de Wouwer et al., 2004; Xue and March, 2025]. Additionally, EPCR serve as molecular target to design treatment strategy against cancer, microvascular thrombosis, malaria and sepsis [Esmon, 2001; 2003; Fink et al., 2013; Xue and March, 2025].

Considering the important role of EPCR in coagulation and inflammation, many studies have been performed to test the anti-EPCR effect of plant and microbial products such as Piperlonguminine (PL), Sulforaphane, Withaferin A (WFA) Aspalathin (Asp), Nothofagin (Not), Diketopiperazine, Rutin and Epi-sesamin (ESM) for the safe and effective treatment strategy for patients with vascular inflammatory diseases [Frommhold et al., 2011; Fink et al., 2013; Ku et al., 2013; 2014a, 2014b, 2014c; 2014d; Kwak et al., 2015; Lee et al., 2016]. Further, in-silico screening and molecular docking studies were performed to understand the molecular interactions between catalytic residues of EPRC with phosphatidylethanolamine (PTY) and di/tripeptides [Chiappori et al., 2009; Chen et al., 2022]. Molecular dynamics simulations of EPCR with phosphatidylethanolamine (PTY), lysophosphatidylcholine (lysoPCh) and phosphatidylcholine (PCh) complexes have been proved to its crucial role in elucidating the catalytic mechanism of EPCR involved in inflammation and coagulation [Chiappori et al., 2010; Prasad and Sen, 2018; Iakhiaev, 2023]. EPCR has importance role in pathological consequences raised by inflammation, however, at present there is no potential EPCR inhibitor is available offering minimal side effects. Therefore, in the present investigations, we have performed structure based virtual screening, molecular docking ADMET property calculations and MD simulations of EPCR in complex with phytochemicals. This study will help to design and potent anti-EPCR drugs molecule to treat diseases caused by severe inflammation.

2. Materials and Methods

2.1. Virtual screening and molecular docking of EPCR

2.1.1. EPCR target preparation

The crystal structure information for EPCR is available at protein data bank (www.rcsb.org). The EPCR crystal structure having highest resolution (1LQV.pdb) was selected for the molecular docking study [Oganesyan et al., 2002].

2.1.2. Ligand data extraction and preparation

The small molecule datasets were downloaded from Indian Medicinal Plants, Phytochemistry and Therapeutics (IMPPAT) and COlleCtion of Open NatUral producTs (COCONUT) chemical databases [Mohanraj et al., 2018; SorZokina et al., 2021]. These databases contain natural products with pharmaceutically and physiologically relevant properties. The IMPPAT 2.0 database contains information about 4,010 Indian medicinal plants, 17,967 phytochemicals, and approximately 1,095 therapeutic applications. Whereas, the COCONUT database represents information of 695,133 natural products. The phytochemicals were downloaded in SDF format and transformed into SMILES notation using Open Babel (v3.1.1) software [O'Boyle et al., 2011]. A similarity-based search was performed against the compound databases using Open Babel, followed by the removal of duplicate structures.

2.1.3. Absorption, Distribution, Metabolism, Excretion, and Toxicity Prediction

The drug-likeness and safety profiles of phytochemicals were analysed by predicting Absorption, Distribution, Metabolism, Excretion, and Toxicity (ADMET) properties using ADMET Lab 3.0 software [Fu et al., 2024]. The compounds were selected based on their Quantitative Estimate of Drug-likeness (QED) scores (>0.67) with higher drug-likeness properties. The Golden Triangle criteria (0 threshold) was used to ensure an optimal balance between molecular weight and lipophilicity that helps to identity potency and pharmacokinetic performance of compounds. The intestinal absorption of compounds was identified by evaluating Caco-2 cell permeability using >-5.15 threshold value. The blood-brain barrier (BBB) permeability predictions (0-0.3) were used to minimize possible side effects of compounds on central nervous system. Ames mutagenicity and hERG channel inhibition tests with 0-0.3 thresholds were performed to assess the toxicological properties of compounds. Additionally, the risk of non-specific binding of compounds to target molecules was eliminated by performing

compounds flagged as Pan-Assay Interference Compounds (PAINS). This comprehensive filtering process ensured the selection of compounds having strong potential with desirable pharmacokinetic profiles and minimized toxicity.

2.1.4. Molecular docking of screened compounds with EPCR

The high-throughput molecular docking of screened compounds with EPCR was performed using AutoDock Vina and Gnina. The binding interactions between the screened ligands with EPCR was assessed using GNINA software [McNutt et al., 2021]. Multi-ligand docking was performed by docking all filtered ligands against the 1LQV structure for EPCR. During docking study, Diclofenac was used as a reference drug molecule. A consensus scoring approach was used to integrate the results obtained from AutoDock Vina v.1.5.7 and GNINA v.1.3 in order to enhance the reliability and accuracy of binding affinity of compounds. This dual-scoring approach enabled more robust and comprehensive analysis of interactions between EPCR and screened compounds. This facilitates the selection of promising drug candidates for further investigation.

2.1.5. MD Simulations and MMGBSA

To understand the effect of water solvent on stability of docked complexes of EPCR and screened drugs, we have performed molecular dynamics simulation using GROMACS v.2025.2 software [Van Der Spoel et al., 2005]. The equilibration protocol consisted of steepest descent energy minimization followed by 200 ps of MD in NVT ensemble at 300 K and 1 ns of MD in NPT ensemble with position restraints applied to EPCR-screened drug complex. Finally, the system was subjected to a production MD run of 200 ns at 300 K temperature and 1 bar pressure under the isothermal-isobaric (NPT) ensemble. A time step of 2 fs was used throughout the simulation with the periodic boundary conditions. The LINCS algorithm was applied to restrain all bonds to a hydrogen atom and permit a time step of 2 fs. [Hess et al., 2008]. The long-range electrostatic interactions were calculated by employing the PME algorithm with a cutoff distance of 1.2 nm. [Essmann et al., 1995]. Binding free energies (ΔG_{bind}) for both the reference ligand and the selected lead compounds (L10, L41, L111, and L114) were calculated by employing the Molecular Mechanics – Generalized Born Surface Area (MM-GBSA) method using Gmx_MMPBSA v.1.6.4.

3. Results and Discussion

3.1. Phytochemical screening and ADMET properties calculations

The COCONUT and IMPPAT databases were carefully filtered to remove duplicates, structurally incomplete entries, and non-plant-derived compounds, yielded approximately 530,654 unique compounds. Further, curated dataset was virtually screened against EPCR. Screening resulted in to 25,419 compounds, which subsequently subjected to ADMET property calculations. ADMET calculations resulted into 278 unique structures for EPCR were retained for downstream analysis.

3.2. Molecular Docking of EPCR and Screened compoundsπ

Molecular docking of EPCR with screened compounds were performed using diclofenac as reference compound. In docking study, only four compounds were formed lowest energy stable docked complexes as compared to Diclofenac (-8.4 and -8.1 Kcal/mol of Autodock and Gnina) (Fig. 1A and Table 1).

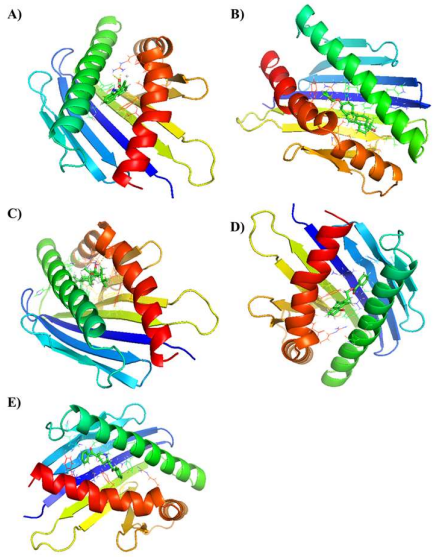

Figure 1: Favourable docked complexes represent position of ligands in the active site pocket of EPCR. A) Docked complex of EPCR with Diclofenac, B) Docked complex of EPCR with L10, C) Docked complex of EPCR with L41, D) Docked complex of EPCR with L111 and E) Docked complex of EPCR with L114.

Table 1: Virtually screened library compounds and their respective binding energy as compared to reference drug.

Library compound	Compound ID	Auto Dock vina binding affinity (Kcal/mol)	Gnina binding affinity (Kcal/mol)
DCF	**Diclofenac**	**-8.4**	**-8.1**
L10	CNP0157233.1	-10.6	-10.8
L41	CNP0294347.1	-10.6	-11.0

L111	CNP0158942.2	-10.7	-11.1
L114	CNP0378567.1	-11.1	-11.0

In this stable docked complex, Diclofenac was placed in the deep catalytic pocket of EPCR where it stabilized by hydrogen bonding, hydrophobic and π-π stacking interactions (Fig. 2 and Table 2). The Tyr72 and Phe164 were involved in strong π-π stacking interactions with Diclofenac. Additionally, hydrophobic contacts between Phe114, Leu161, and Phe164 from active site pocket provide structural stability to docking complex. The compounds L10, L41, L111 and L114 were produced lowest energy stable docked complexes as compared to Diclofenac (Table 1). The compound L10 was forming stable docked complex with EPCR having -10.6/-10.8 Kcal/mol binding energy of Autodock/Gnina (Fig. 1B and Tables 1-2). This docked complex was stabilized by hydrophobic contacts between Gln75, Phe76, Leu79, Val80, Ile95, Val116, Trp133, Thr147, Leu151, Thr157, Leu161, and Phe164 residues from active site pocket and L10 (Table 2). Next stable docked complex was produced by compound L41 with EPCR having binding energy of -10.6/-11.0 Kcal/mol produced by Autodock/Gnina (Fig. 1C and Table 2). In this stable complex, the L41 was involved in strong hydrogen bonding interaction with Arg156 by maintaining 3.59 Å distance (Fig. 1C and Table 2). Additional stabilization of docked complex was expected from hydrophobic interactions between Tyr72, Gln75, Phe76, Leu79, Val80, Val83, Ile95, Phe114, Phe123, Trp133, Thr147, Leu151, Phe164 and L41 (Table 2). Next lowest energy favourable docked complex was produced between EPCR and L111 having binding energy -10.7/-11.1 Kcal/mol (Figs. 1D and 2D; Tables 1-2). This docked complex was stabilized by hydrogen as well as π-π stacking interactions (Figs. 1D, 2D and Tables 1-2). The Arg156 was participated in strong hydrogen bonding interaction with L111 by maintaining distance 3.12 Å. The π-π stacking interaction was observed between Phe164 and L111 was one of the crucial factors in stabilization of docked complex of L111 and EPCR (Fig. 2D).

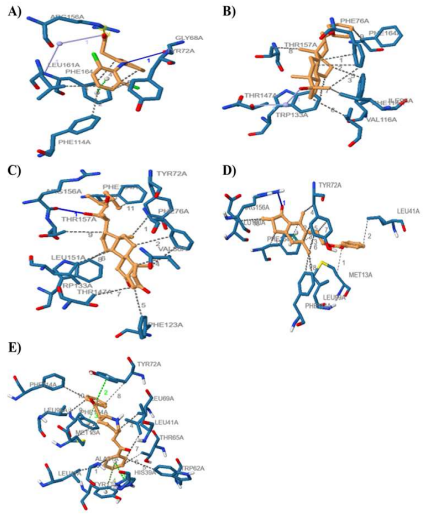

Figure 2: Molecular interactions between docked complexes of A) Docked complex of EPCR with Diclofenac, B) Docked complex of EPCR with L10, C) Docked complex of EPCR with L41, D) Docked complex of EPCR with L111 and E) Docked complex of EPCR with L114.

Table 2: Geometrical parameters for hydrogen bonding, π-π stacking and hydrophobic interactions from stable docked complexes.

Docked complexes	**Atoms involved in H-bonds**	**Atoms involved in π-π stacking**	**Distance in Å**	**Angles in Degree**	**Ref. Fig.**
EPCR with Diclofenac	Phe114, Leu161, Phe164 (Hydrophobic Interactions)	Tyr72…. Diclofenac Phe164 …. Diclofenac	4.30 3.81	- -	1A
EPCR with L10	Gln75, Phe76, Leu79, Val80, Ile95, Val116, Trp133, Thr147, Leu151, Thr157, Leu161, Phe164			-	
EPCR with L41	Arg156 …….L41 Tyr72, Gln75, Phe76,	-	3.59	100.08	

	Leu79, Val80, Val83, Ile95, Phe114, Phe123, Trp133, Thr147, Leu151, Phe164				
EPCR with L111	Arg156 …….L111 - Met13, Leu41, Tyr72, Leu99, Phe114, Glu160, Phe164,	- Phe164	3.12 3.74	139 .08 -	
EPCR with L114	- - - - Leu11, Met13, Ala31, Leu41, Trp62, Thr65, Leu69, Tyr72, Leu99, Phe114	His39… …L114 Tyr72… …L114 Phe164 …..L114 Tyr172 ……L114	3.80 3.79 4.03 5.10	- - - -	

The next lowest energy (-11.1/-11.0 Kcal/mol) stable docked complex was produced by L114 with EPCR (Figs. 1E and 2E; Tables 1-2). In this stable complex, L114 was positioned in the deep catalytic pocket of EPCR, where it was noticeably stabilized by π-π stacking interactions between His39……L114, Tyr72……L114, Phe164…..L114, and Tyr72……L114 (Table 2). The hydrophobic interactions from Leu11, Met13, Ala31, Leu41, Trp62, Thr65, Leu69, Tyr72, Leu99, Phe114 residues provide additional structural stability to the docked complex between EPCR and L114 (Fig. 2E).

The docking study helps to understand the molecular mechanism of catalytic inhibition of EPCR by Diclofenac, L10, L41, L111 and L114 compounds. These complexes were further subjected for molecular dynamics simulations.

3.3. Molecular Dynamics Simulation Analysis

Molecular dynamics simulation was performed to get structural insight into the conformational dynamics of EPCR and to understand the inhibition mechanism of human EPCR by Diclofenac, L10, L41, L111 and L114. The dynamic stability of the EPCR and ligands complexes were evaluated by calculating the root mean square deviation (RMSD) of Cα atoms of the protein backbone throughout the 200 ns of simulation and shown in Figure 3A. All complexes were stabilized throughout the simulations, evidenced by RMSD values ranges between 0.1 to 0.2 nm (Fig. 3A). The reference drug Diclofenac and screened drugs L111 and L114 were prominently stabilized over 200 ns of simulations. The slight fluctuations in RMSD were noticed in L41 and EPCR complex, whereas L10 was slightly destabilized after 125 ns of simulation period. The conformational dynamics of ligands were also tested during MD simulations (Fig. 3B). All ligands were stabilized in catalytic pocket of EPCR, where L41 and l114 were mostly stabilized in complex as compared to Diclofenac. The calculated RMSF values for all the simulated complexes were below 0.2 nm which signifies the good stability for simulated complexes of screened compounds and EPCR during simulation (Fig. 3C). The catalytic residues involving in hydrogen bonding and hydrophobic interactions with Diclofenac, L10, L41, L111 and L114 compounds showed the least fluctuations throughout 200 ns of simulations which is evident by the < 0.1 nm RMSF value of respective residues (Fig. 3C). Further, the structural stability of simulated complexes of EPCR and Diclofenac, L10, L41, L111 and L114 compounds was assessed by calculating the radius of gyration (Rg) (Fig. 3D). The Rg predicts the compactness of the protein owing to the spatial arrangement of secondary structures. The Rg values 1.62 nm to 1.8 nm of EPCR represent the compactness of EPCR during simulations due to the stable behaviour of secondary structures.

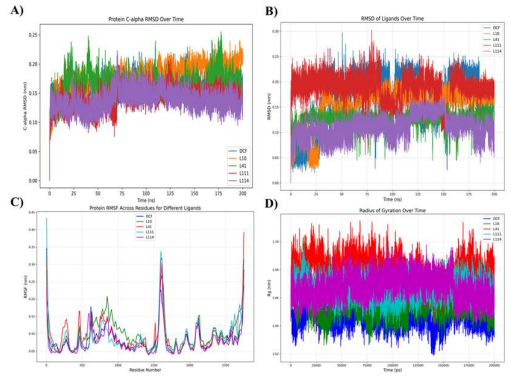

Figure 3: A) RMSD fluctuation of Cα atoms of the EPCR in presence of Diclofenac, L10, L41, L111 and L114 complexes during 200 ns of MD simulation study. B) RMSD of ligands in presence of EPCR during 200 ns, C) RMSF fluctuations for EPCR residues.

The presence of hydrogen bonds from simulated complexes of EPCR with DCF, L10, L41, L111 and L114 were calculated for 200 ns of simulation period (Fig. 4). The stability of Diclofenac and EPCR complex during simulation was supported by the presence of higher number of hydrogen bonds between EPCR and Diclofenac

(Fig. 4A). In L10 and EPCR complex less hydrogen bonds were observed during simulation as compared to Diclofenac (Fig. 4B). In contrast the L41 was forming more hydrogen bonding interactions as compared to L10 but less than Diclofenac (Fig. 4C). The hydrogen bonding interactions present between L111 and EPCR were less as compared to Diclofenac and L10, and L41 (Fig. 4D). Further, the L114 was forming stable complex with EPCR which was supported by the presence of hydrogen bonds maintained during simulation (Fig. 4E). The stability of simulated complexes and interactions of catalytic residues with ligand molecules represented by the RMSD and RMSF were strongly supported by the hydrogen bonds maintained during MD simulations. Hydrogen bonding interactions are the key stabilizing factor in protein-ligand complexes and supported by our MD simulation results.

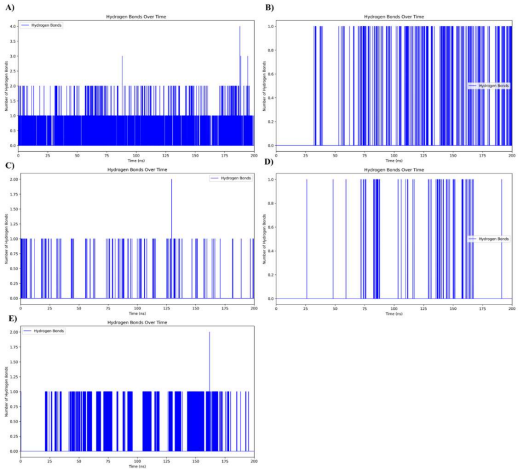

Figure 4: Depicted the presence of H-bonds from simulated complexes of A) EPCR and Diclofenac, B) EPCR and L10, C) EPCR and L41, D) EPCR and L111 and E) EPCR and L114

3.4. Binding free energy calculations of simulated complexes of EPCR with Diclofenac, L10, L41, L111 and L114 using MMGBSA Analysis

Further energetic components of simulated complex and energetic components per residue of EPCR with Diclofenac were calculated (Figs. 5A-4B). The pattern of both energetic components is similar and showed stable behaviour throughout 200 ns of simulation period. The figure 4C and 4D showed the energetic components of residues from catalytic site of EPCR and Diclofenac. The Tyr72 and Arg156 has good and stable energetic components because of its involvement in π-π stacking interactions with Diclofenac (Fig. 5C and 4D). The low but significant energetic contribution toward stable complex was generated by Leu161 and Phe164 due to their hydrophobic interactions with Diclofenac. Figure 4E and 4F depicted energetically and structurally stable 2D and 3D free energy landscape of simulated complex of ECPR with Diclofenac. This supported the energetic contribution of interacting residues with Diclofenac during simulation.

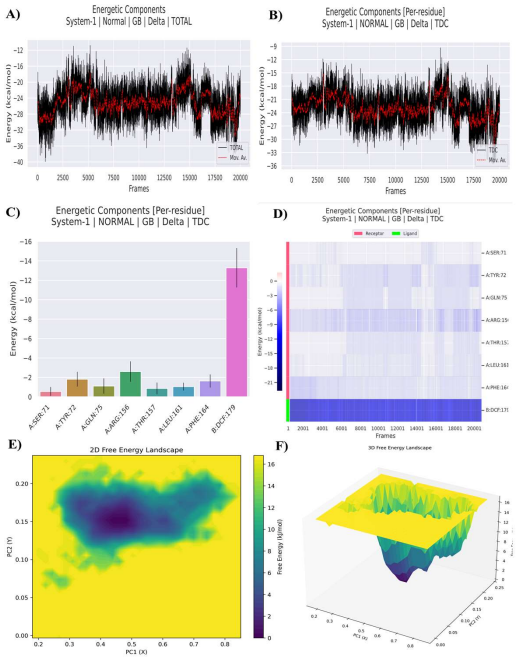

Figure 5: Calculated energetic components of A) Simulated complex of Diclofenac with EPCR, B) Energetic components of per residues of simulated complex, C) Energetic contribution of residues interacting with Diclofenac, D) Heatmap represent energetic relation of interacting residues with Diclofenac, E) 2D-free energy landscape of simulated complex of EPCR with Diclofenac, and F) 3D- free energy landscape of simulated complex of EPCR with Diclofenac.

Energetic components of EPCR with L10 simulated complex and their per residue contribution in stability of complex was depicted in figure 5A and 5B. A stable energetic behaviour was observed for EPCR with L10. The Val118 and Phe123 residues were energetically contributed significantly in stability of simulated complex of EPCR and L10 (Figs. 6C and 5D). The low energetic contribution of Leu79 and Val80 residues in stability of complex was also expected based on their energy content during simulation. The one major and two small macrostates of simulated complex were observed during simulation. The major microstate was energetically more stable as compared to other two macrostates. This suggested the stable behaviour of EPCR with L10 during simulation. Similar pattern was observed in 2D and 3D free energy landscape of simulated complex.

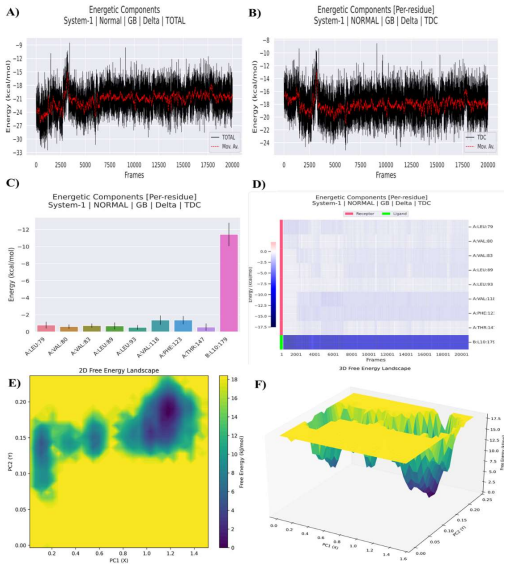

Figure 6: Calculated energetic components of A) Simulated complex of L10 with EPCR, B) Energetic components of per residues of simulated complex, C) Energetic contribution of residues interacting with L10, D) Heatmap represent energetic relation of interacting residues with L10, E) 2D-free energy landscape of simulated complex of EPCR with L10, and F) 3D- free energy landscape of simulated complex of EPCR with L10.

Figures 7A and 7B showed energetic components of EPCR with L41 simulated complex and their per residue contribution in stability during 200 ns. Stable energetic behaviour was observed for EPCR with L41 between -28 to -36 Kcal/mol. The Tyr72, Gln75, and Leu79 residues were involved in providing structural stability to EPCR and L41 complex during simulation (Figs. 7C and 7D). Here also, the simulated complex was highly stable during simulation which is indicated by 2D and 3D free energy landscape diagram (Figs. 7E and 7F).

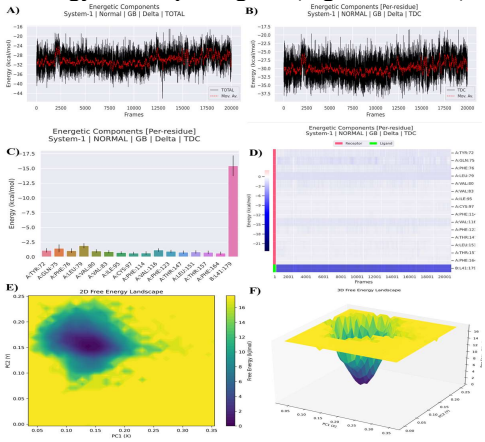

Figure 7: Calculated energetic components of A) Simulated complex of L41 with EPCR, B) Energetic components of per residues of simulated complex, C) Energetic contribution of residues interacting with L41, D) Heatmap represent energetic relation of interacting residues with L41, E) 2D-free energy landscape of simulated complex of EPCR with L41, and F) 3D- free energy landscape of simulated complex of EPCR with L41.

Similarly, figures 8A and 8B showed energetic components of EPCR with L111 simulated complex and their per residue contribution in stability of complex during 200 ns. Stable energetic behaviour was observed for EPCR with L111 between -22 to -30 Kcal/mol. The Phe164 was participated in π-π stacking interaction with L111 during MD simulation (Fig. 8C and 8D). The Met13, Tyr72, and Leu99 residues were significantly involved in hydrophobic interactions with L111 and supported by energetic components. Further two macrostates separated by slight conformational changes were observed which were supported by 2D and 3D free energy landscapes (Figs. 8E and 8F).

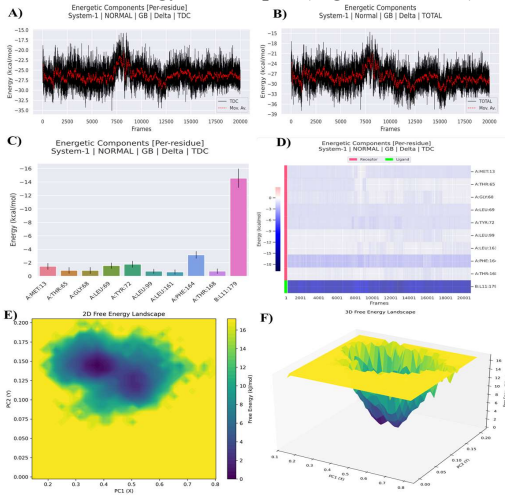

Figure 8: Calculated energetic components of A) Simulated complex of L111 with EPCR, B) Energetic components of per residues of simulated complex, C) Energetic contribution of residues interacting with L111, D) Heatmap represent energetic relation of interacting residues with L111, E) 2D-free energy landscape of simulated complex of EPCR with L111, and F) 3D- free energy landscape of simulated complex of EPCR with L111.

Furthermore, the energetic components per residues involved in stability of EPCR and L114 complex during simulations were calculated and showed stable behaviour ranging from -25 to -35 Kcal/mol (Figs. 9A and 9B). The energetic stability of EPCR and L114 simulated complex was supported by in π-π stacking interactions resulted from His39, Tyr72, Phe164, and Tyr172 residues (Figs. 9C and 9D). The energetic contribution of Met13, Ala31, Leu41, Thr65, Leu69, Tyr72, and Leu99 were supported by hydrophobic interactions were observed in docking study. Interestingly, single major stable macrostate was observed for the simulated complex of EPCR and L114.

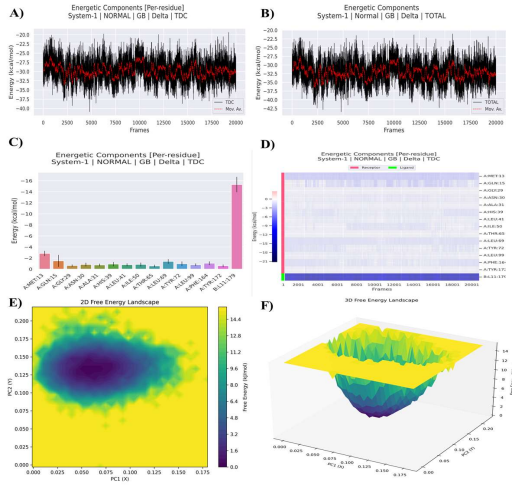

Figure 9: Calculated energetic components of A) Simulated complex of L114 with EPCR, B) Energetic components of per residues of simulated complex, C) Energetic contribution of residues interacting with L114, D) Heatmap represent energetic relation of interacting residues with L114, E) 2D-free energy landscape of simulated complex of EPCR with L114, and F) 3D- free energy landscape of simulated complex of EPCR with L114.

Overall simulated complexes and their calculated energy components per residues supported by hydrogen binding, π-π stacking and hydrophobic interactions.

The binding mechanism and binding proficiency of Diclofenac, L10l L41, L111 and L114 toward the EPCR were investigated by calculating the MM-PBSA (Table 3). Total binding energy ($\Delta G_{binding}$) of Diclofenac-EPCR, L10-EPCR, L41-EPCR, L111-EPCR and L114-EPCR are -25.18 ± 0.03, -25.18 ± 0.03, -30.15 ± 0.02, -28.19 ± 0.02 and -32.20 ± 0.02, respectively. Among them, L114 (-32.20 ± 0.02 kcal/mol) demonstrated the most stable and energetically favourable affinity, followed by L41 (-30.15 ± 0.02 kcal/mol) and L111 (-28.19 ± 0.02 kcal/mol).

Table 3: Calculated MMBPSA for simulated complexes of EPCR with Diclofenac, L10, L41, L11, and L114.

Sr.no	Ligand	ΔE_vdw	ΔE_ele	ΔG_polar	ΔG_nonpolar	ΔG_bind (kcal/mol)
1.	**L114**	-42.42	-7.41	23.84	-6.20	**-32.20 ± 0.02**
2.	**L41**	-52.79	-6.40	36.53	-7.50	**-30.15 ± 0.02**
3.	**L111**	-39.47	-1.58	18.12	-5.25	**-28.19 ± 0.02**
4.	**DCF**	-32.32	-5.36	16.53	-4.03	**-25.18 ± 0.03**
5.	**L10**	-40.33	-0.73	25.54	-5.68	**-21.20 ± 0.02**

These values are significantly better than the reference compound DCF (-25.18 ± 0.03 kcal/mol), suggesting enhanced binding efficiency of the screened phytocompounds. Moreover table 4 showed compound common name and 2D molecular structures of screened phytochemicals which were tested for their binding affinity by performing docked and MD simulations.

Table 4: Represent compound names and their 2D structure.

Sr. no.	Library compound	Compound ID	Compound Name	Molecular 2D structures
1.	DCF	-	Diclofenac	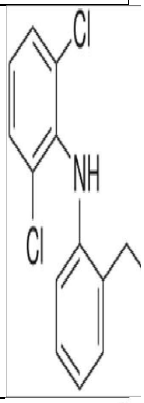
2.	L10	CNP0157233.1	Penmesterol	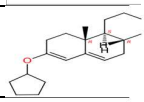
3.	L41	CNP0294347.1	3-Dehydrotesterone	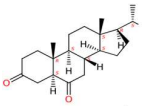
4.	L111	CNP0158942.2	2-[(2*S*)-2,4,6-trimethyl-3-oxo-indan-5-yl]ethyl benzoate	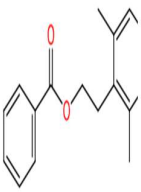
5.	L114	CNP0378567.1	Norlobelanine	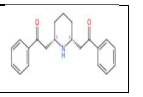

Conclusion:

The present study highlights the potential of phytochemicals as promising EPCR inhibitors for managing inflammation-related disorders. By combining virtual screening, ADMET evaluation, molecular docking, molecular dynamics simulations, and MM-GBSA analysis, several natural compounds were assessed for their ability to interact with EPCR. Among the screened molecules Penmesterol, 3-Dehydroteasterone, 2-[(2*S*)-2,4,6-trimethyl-3-oxo-indan-5-yl]ethyl benzoate and Norlobelanine showed stronger binding affinity than the reference drug diclofenac and formed stable interactions with important residues within the EPCR binding pocket. The molecular dynamics simulations confirmed that these complexes remained stable throughout the 200 ns simulation period, supported by favourable structural and energetic behaviour. Binding free-energy calculations further demonstrated that Norlobelanine, followed by 3-Dehydroteasterone and 2-[(2*S*)-2,4,6-trimethyl-3-oxo-indan-5-yl]ethyl benzoate exhibited stronger and more stable interactions with EPCR compared to diclofenac. Overall, these findings suggest that the selected phytochemicals, particularly Norlobelanine, may serve as potential lead molecules for developing new anti-inflammatory therapies targeting EPCR. While the computational results are encouraging, further in vitro and in vivo studies will be necessary to validate their biological activity and therapeutic potential.

References:

Beaulieu LM, Church FC. Activated protein C promotes breast cancer cell migration through interactions with EPCR and PAR-1. *Exp Cell Res.* 2007;313(4):677-687. doi:10.1016/j.yexcr.2006.11.019

Biguzzi E, Franchi F, Bucciarelli P, Colombo M, Romeo R. Endothelial protein C receptor plasma levels increase in chronic liver disease, while thrombomodulin plasma levels increase only in hepatocellular carcinoma. *Thromb Res.* 2007;120(2):289-293. doi:10.1016/j.thromres.2006.09.009

Chen Y, Guo Y, Liu Y, Zhang C, Huang F, Chen L. Identification of Di/Tripeptide(s) With Osteoblasts Proliferation Stimulation Abilities of Yak Bone Collagen by *in silico* Screening and Molecular Docking. *Front Nutr.* 2022;9:874259. doi:10.3389/fnut.2022.874259

Chiappori F, D'Ursi P, Merelli I, Milanesi L, Rovida E. In silico saturation mutagenesis and docking screening for the analysis of protein-ligand interaction: the Endothelial Protein C Receptor case study. *BMC Bioinformatics.* 2009;10(Suppl 12):S3. doi:10.1186/1471-2105-10-S12-S3

Chiappori F, Merelli I, Milanesi L, Rovida E. Exploring the role of the phospholipid ligand in endothelial protein C receptor: a molecular dynamics study. *Proteins.* 2010;78(12):2679-2690. doi:10.1002/prot.22782

Esmon CT. Protein C anticoagulant pathway and its role in controlling microvascular thrombosis and inflammation. *Crit Care Med.* 2001;29(7 Suppl):S48-S52. doi:10.1097/00003246-200107001-00018

Esmon CT. Coagulation and inflammation. *J Endotoxin Res.* 2003;9(3):192-198. doi:10.1179/096805103125001603

Esmon CT. Crosstalk between inflammation and thrombosis. *Maturitas.* 2004;47(4):305-314. doi:10.1016/j.maturitas.2003.10.015

Esmon CT. Inflammation and the activated protein C anticoagulant pathway. *Semin Thromb Hemost.* 2006;32(Suppl 1):49-60. doi:10.1055/s-2006-939554

Essmann U, Perera L, Berkowitz ML, Darden T, Lee H, Pedersen LG. A smooth particle mesh Ewald method. *J Chem Phys.* 1995;103:8577-8593. doi:10.1063/1.470117

Fink K, Busch HJ, Bourgeois N, et al. Mac-1 directly binds to the endothelial protein C-receptor: a link between the protein C anticoagulant pathway and inflammation? *PLoS One.* 2013;8(2):e53103. doi:10.1371/journal.pone.0053103

Frommhold D, Tschada J, Braach N, et al. Protein C concentrate controls leukocyte recruitment during inflammation and improves survival during endotoxemia after efficient in vivo activation. *Am J Pathol.* 2011;179(5):2637-2650. doi:10.1016/j.ajpath.2011.07.023

Fu L, Shi S, Yi J, et al. ADMETlab 3.0: an updated comprehensive online ADMET prediction platform enhanced with broader coverage, improved performance, API functionality and decision support. *Nucleic Acids Res.* 2024;52(W1):W422-W431. doi:10.1093/nar/gkae236

Fukudome K, Esmon CT. Identification, cloning, and regulation of a novel endothelial cell protein C/activated protein C receptor. *J Biol Chem.* 1994;269(42):26486-26491.

Gleeson EM, O'Donnell JS, Preston RJ. The endothelial cell protein C receptor: cell surface conductor of cytoprotective coagulation factor signaling. *Cell Mol Life Sci.* 2012;69(5):717-726. doi:10.1007/s00018-011-0825-0

Heng W, Mu CY, Chen C, Huang JA, Wang ZY. Endothelial cell protein C receptor (EPCR) is expressed by lung carcinoma and correlated with clinical parameters. *Clin Lab.* 2013;59(3-4):375-380. doi:10.7754/clin.lab.2012.120214

Hess B. P-LINCS: A Parallel Linear Constraint Solver for Molecular Simulation. *J Chem Theory Comput.* 2008;4(1):116-122. doi:10.1021/ct700200b

Iakhiaev A. The structural basis of the EPCR-APC complex induced biased PAR1 signaling. *BioRxiv.* 2023.

Ku SK, Han MS, Bae JS. Sulforaphane inhibits endothelial protein C receptor shedding in vitro and in vivo. *Vascul Pharmacol.* 2014b;63(1):13-18. doi:10.1016/j.vph.2014.06.002

Ku SK, Han MS, Bae JS. Withaferin A is an inhibitor of endothelial protein C receptor shedding in vitro and in vivo. *Food Chem Toxicol.* 2014;68:23-29. doi:10.1016/j.fct.2014.03.009

Ku SK, Kim JA, Bae JS. Piperlonguminine downregulates endothelial protein C receptor shedding in vitro and in vivo. *Inflammation.* 2014a;37(2):435-442. doi:10.1007/s10753-013-9756-2

Ku SK, Lee IC, Han MS, Bae JS. Inhibitory effects of rutin on the endothelial protein C receptor shedding in vitro and in vivo. *Inflammation.* 2014;37(5):1424-1431. doi:10.1007/s10753-014-9866-5

Ku SK, Lee W, Yoo H, Han CK, Bae JS. Inhibitory effects of epi-sesamin on endothelial protein C receptor shedding in vitro and in vivo. *Inflamm Res.* 2013;62(10):895-902. doi:10.1007/s00011-013-0648-6

Kwak S, Han MS, Bae JS. Aspalathin and nothofagin from rooibos (*Aspalathus linearis*) inhibit endothelial protein C receptor shedding in vitro and in vivo. *Fitoterapia.* 2015;100:179-186. doi:10.1016/j.fitote.2014.12.002

Lee W, Ku SK, Choi H, Bae JS. Inhibitory effects of three diketopiperazines from marine-derived bacteria on endothelial protein C receptor shedding in human endothelial cells and mice. *Fitoterapia.* 2016;110:181-188. doi:10.1016/j.fitote.2016.03.016

Li W, Zheng X, Gu J, et al. Overexpressing endothelial cell protein C receptor alters the hemostatic balance and protects mice from endotoxin. *J Thromb Haemost.* 2005;3(7):1351-1359. doi:10.1111/j.1538-7836.2005.01385.x

Lust M, Vulcano M, Danese S. The protein C pathway in inflammatory bowel disease: the missing link between inflammation and coagulation. *Trends Mol Med.* 2008;14(6):237-244. doi:10.1016/j.molmed.2008.03.005

McNutt AT, Francoeur P, Aggarwal R, et al. GNINA 1.0: molecular docking with deep learning. *J Cheminform.* 2021;13(1):43. doi:10.1186/s13321-021-00522-2

Mohan Rao LV, Esmon CT, Pendurthi UR. Endothelial cell protein C receptor: a multiliganded and multifunctional receptor. *Blood.* 2014;124(10):1553-1562. doi:10.1182/blood-2014-05-578328

Mohanraj K, Karthikeyan BS, Vivek-Ananth RP, et al. IMPPAT: A curated database of Indian Medicinal Plants, Phytochemistry And Therapeutics. *Sci Rep.* 2018;8(1):4329. doi:10.1038/s41598-018-22631-z

Moxon CA, Wassmer SC, Milner DA Jr, et al. Loss of endothelial protein C receptors links coagulation and inflammation to parasite sequestration in cerebral malaria in African children. *Blood.* 2013;122(5):842-851. doi:10.1182/blood-2013-03-490219

O'Boyle NM, Banck M, James CA, Morley C, Vandermeersch T, Hutchison GR. Open Babel: An open chemical toolbox. *J Cheminform.* 2011;3:33. doi:10.1186/1758-2946-3-33

Oganesyan V, Oganesyan N, Terzyan S, et al. The crystal structure of the endothelial protein C receptor and a bound phospholipid. *J Biol Chem.* 2002;277(28):24851-24854. doi:10.1074/jbc.C200163200

Prasad R, Sen P. Phosphatidylcholine in the groove of endothelial cell protein C receptor (EPCR) regulates EPCR conformation and protein C recognition. *Integr Biol (Camb).* 2018;10(11):696-704. doi:10.1039/c8ib00115d

Scaldaferri F, Sans M, Vetrano S, et al. Crucial role of the protein C pathway in governing microvascular inflammation in inflammatory bowel disease. *J Clin Invest.* 2007;117(7):1951-1960. doi:10.1172/JCI31027

Sorokina M, Merseburger P, Rajan K, Yirik MA, Steinbeck C. COCONUT online: Collection of Open Natural Products database. *J Cheminform.* 2021;13(1):2. doi:10.1186/s13321-020-00478-9

Stearns-Kurosawa DJ, Kurosawa S, Mollica JS, Ferrell GL, Esmon CT. The endothelial cell protein C receptor augments protein C activation by the thrombin-thrombomodulin complex. *Proc Natl Acad Sci U S A.* 1996;93(19):10212-10216. doi:10.1073/pnas.93.19.10212

Van de Wouwer M, Collen D, Conway EM. Thrombomodulin-protein C-EPCR system: integrated to regulate coagulation and inflammation. *Arterioscler Thromb Vasc Biol.* 2004;24(8):1374-1383. doi:10.1161/01.ATV.0000134298.25489.92

Van Der Spoel D, Lindahl E, Hess B, Groenhof G, Mark AE, Berendsen HJ. GROMACS: fast, flexible, and free. *J Comput Chem.* 2005;26(16):1701-1718. doi:10.1002/jcc.20291

Weiler H. Regulation of inflammation by the protein C system. *Crit Care Med.* 2010;38(2 Suppl):S18-S25. doi:10.1097/CCM.0b013e3181c9cbb5

Xue M, March L. Endothelial Protein C Receptor: A Multifunctional Mediator in the Pathophysiology of Rheumatoid Arthritis. *Cells.* 2025;14(7):485. doi:10.3390/cells14070485

Xue M, Shen K, McKelvey K, et al. Endothelial protein C receptor-associated invasiveness of rheumatoid synovial fibroblasts is likely driven by group V secretory phospholipase A2. *Arthritis Res Ther.* 2014;16(1):R44. doi:10.1186/ar4473